Surveying the $N = 40$ island of inversion with new manganese masses

S. Naimi,[1,2] G. Audi,[1] D. Beck,[3] K. Blaum,[4,5] Ch. Böhm,[4,5] Ch. Borgmann,[4,5] M. Breitenfeldt,[6,*] S. George,[4,7,†] F. Herfurth,[3] A. Herlert,[8,‡] A. Kellerbauer,[4] M. Kowalska,[8] D. Lunney,[1] E. Minaya Ramirez,[1,§] D. Neidherr,[4,7,§] M. Rosenbusch,[6] L. Schweikhard,[6] R. N. Wolf,[6] and K. Zuber[9]

[1]*CSNSM-IN2P3-CNRS, Université de Paris Sud, 91405 Orsay, France*
[2]*Nishina Accelerator-based Research Center, RIKEN, 2-1 Hirosawa, Wako, Saitama 351-0198, Japan*
[3]*GSI Helmholtzzentrum für Schwerionenforschung GmbH, Planckstraße 1, 64291 Darmstadt, Germany*
[4]*Max-Planck-Institut für Kernphysik, Saupfercheckweg 1, 69117 Heidelberg, Germany*
[5]*Fakultät für Physik und Astronomie, Ruprecht-Karls-Universität, 69120 Heidelberg, Germany*
[6]*Institut für Physik, Ernst-Moritz-Arndt-Universität, 17487 Greifswald, Germany*
[7]*Institut für Physik, Johannes Gutenberg-Universität, 55128 Mainz, Germany*
[8]*CERN, Physics Department, 1211 Geneva 23, Switzerland*
[9]*Institut für Kern- und Teilchenphysik, Technische Universität, 01069 Dresden, Germany*

(Received 29 October 2011; revised manuscript received 14 May 2012; published 20 July 2012)

High-precision mass measurements of neutron-rich $^{57-66}$Mn and $^{61-63}$Fe isotopes are reported. The new mass surface shows no shell closure at $N = 40$. In contrast, there is an increase of the two-neutron separation energy at $N = 38$. This behavior is consistent with the onset of collectivity due to the occupation of intruder states from higher orbits, in analogy with the well known "island of inversion" around $N = 20$. Our results indicate that the neutron-rich Mn isotopes, starting from ^{63}Mn, are most likely within the new island of inversion. From the new mass surface, we evaluate the empirical proton-neutron interaction and the pairing gap, both playing a significant role in the structural changes in this region.

DOI: 10.1103/PhysRevC.86.014325 PACS number(s): 21.10.Dr, 21.10.Re, 21.10.Gv

I. INTRODUCTION

The discovery of the "island of inversion" around ^{32}Mg and the vanishing of the $N = 20$ shell closure has profoundly affected our understanding of nuclear structure [1–7]. Dramatic changes in shell structure occur in this region, where nucleons occupy intruder states across the shell at low excitation energy and in the ground state. The case of $N = 20$ is an important benchmark for the disappearance of magic numbers in heavier nuclides. The existence of a new island of inversion around $N = 40$ has been discussed in light of experimental results [8–10] as well as theoretical studies [11,12]. The increase of collectivity observed around $N = 40$ is thought to be due to the neutron occupation of intruder states from a higher shell similar to the island of inversion around $N = 20$. While $N = 40$ is not considered a shell closure in the shell model, its magicity was proposed by Bernas *et al.* [13] from the discovery of a high-lying first excited state in ^{68}Ni, confirmed by the measurements of Broda *et al.* [14]. The closed-shell nature of $N = 40$ was supported later from the measurement of the reduced transition probability $B(E2; 2^+ \rightarrow 0^+)$ of ^{68}Ni, which yielded the smallest $B(E2)$ value of all semi-magic nuclides [15]. However, none of the neighboring nuclides show similar behavior and, instead, all show an increase of collectivity attributed to the occupation of a neutron intruder orbital ($\nu g_{9/2}$) [8,9,16,17]. Moreover, the two-neutron separation energies show a remarkably smooth behavior in the $N = 40$ region for Ni, Cu, Ga [18], and Fe isotopes [19], in marked contrast to the suggested magicity of $N = 40$ where a sudden drop in S_{2n} values would be expected.

The $N = 40$ shell closure is known to be very weak, especially below $Z = 28$ where the proton-neutron interaction starts to play an important role in the nucleon orbital occupation ($\nu f_{5/2}$ and $\nu g_{9/2}$) and, hence, the total binding energy. β-decay studies on neutron-rich Ti, V, Cr, Mn, and Fe isotopes [20–26] show that the allowed Gamow-Teller β decay is dominated by the $\nu f_{5/2} \rightarrow \pi f_{7/2}$ transition. The occupation of the intruder neutron orbital $\nu g_{9/2}$ depends strongly on the proton-neutron interaction. This interaction between the $\nu f_{5/2}$ orbital and the $\pi f_{7/2}$ orbital is weaker when protons are removed from the $\pi f_{7/2}$ orbital. As a consequence, the $\nu f_{5/2}$ orbital moves closer to the $\nu g_{9/2}$ orbital where the pairing effect favors pair scattering to a higher orbit [15,24,27–29]. As was stressed in Ref. [24], high-precision mass measurements were missing to evaluate more quantitatively the influence of the proton-neutron interaction on the occupation of these orbitals.

In this work, mass measurements of neutron-rich manganese and iron isotopes ($^{57-66}$Mn, $^{61-63}$Fe) performed with the ISOLTRAP mass spectrometer are presented. The $N = 40$ shell closure is discussed in light of different mass derivatives using the new Mn binding energies: the two-neutron separation energy and the empirical shell gap. Finally, we discuss the pairing gap and the empirical proton-neutron interaction that

*Present address: Instituut voor Kern- en Stralingsfysica, B-3001 Leuven, Belgium.
†Present address: NSCL, Department of Physics and Astronomy, Michigan State University, MI 48824, East Lansing, USA.
‡Present address: FAIR GmbH, Planckstr. 1, 64291 Darmstadt, Germany.
§Present address: GSI Helmholtzzentrum für Schwerionenforschung GmbH, Planckstraße 1, 64291 Darmstadt, Germany.

are calculated from the new mass surface, and their implication in the new island of inversion.

II. EXPERIMENTAL SETUP

A. ISOLDE and ISOLTRAP setup

The measurements were performed using the mass spectrometer ISOLTRAP [30] installed at the online isotope separator ISOLDE at CERN [32]. To produce the Mn isotopes a uranium-carbide (UC_x) target was bombarded by a 1.4-GeV proton beam from CERN's Proton Synchrotron Booster (PSB). The resulting atoms were ionized using the Resonance Ionization Laser Ion Source (RILIS) [33,34]. The ions were accelerated and transported through the General Purpose Separator (GPS), which was operated with a resolving power of $m/\Delta m = 800$, and then sent to the ISOLTRAP experiment, shown in Fig. 1.

ISOLTRAP consists of three main parts: a radio-frequency quadrupole (RFQ), a cylindrical preparation Penning trap, and a hyperbolic precision Penning trap. The RFQ and the first Penning trap are used to cool and prepare the beam while the second Penning trap is used for high-precision mass measurements. The ISOLDE quasi-continuous beam is stopped and accumulated in the linear RFQ [35]. The ions are

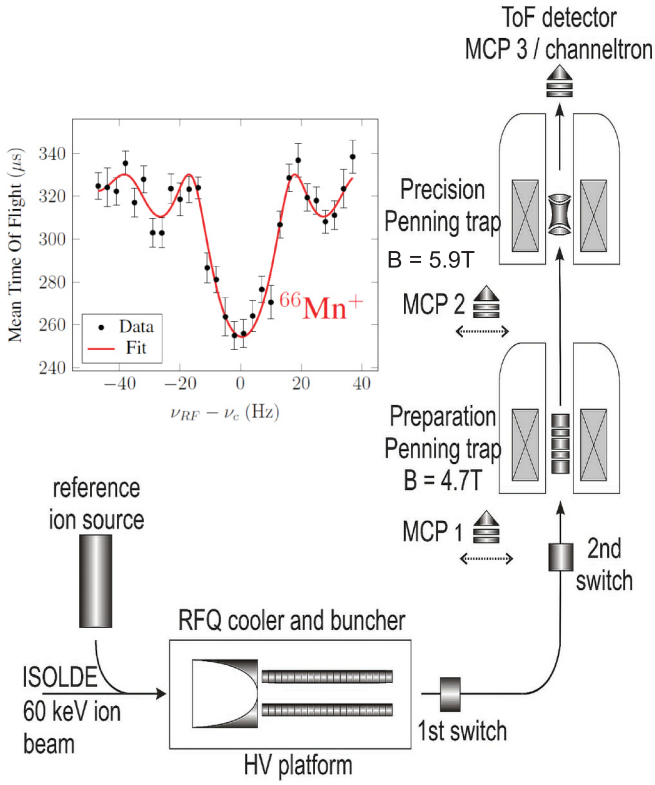

FIG. 1. (Color online) ISOLTRAP experimental setup [30]. The ISOLDE beam is stopped and cooled in the RFQ cooler and buncher, transported to the cylindrical preparation Penning trap for isobaric purification, then to the hyperbolic precision Penning trap for the mass measurement. On the top left is shown one of the $^{66}Mn^{+}$ time-of-flight ion cyclotron resonances recorded in the precision Penning trap along with the fit of the theoretical line-shape [31].

cooled by energy loss due to collisions with helium buffer gas present in the RFQ. After an accumulation time of a few milliseconds the ion bunch is ejected from the RFQ and transferred to the first Penning trap. Here, the mass-selective helium buffer-gas cooling technique [36] is used for isobaric cleaning with high resolving power. The purified beam is then transferred to the hyperbolic precision trap placed in ultrahigh vacuum where the mass measurement is performed. The mass is determined by measuring the ion's cyclotron frequency $\nu_c = qB/(2\pi m)$ where q and m are the charge and the mass of the ion, respectively. The magnetic field strength B is calibrated repeatedly by measuring the cyclotron frequency of ions with well known mass. For this purpose a stable-alkali reference ion source is installed at ISOLTRAP in front of the RFQ. For the present experiment $^{39}K^{+}$ and $^{85}Rb^{+}$ were used as reference ions. Stable ion beams from ISOLDE can be also used for the same purpose.

B. Penning traps and mass measurement procedure

Solving the equations of motion of a charged particle in a Penning trap gives three harmonic oscillator modes: one in the axial direction with the frequency ν_z and two in the radial plane, with the modified cyclotron frequency ν_+ and the magnetron frequency ν_-. In an ideal Penning trap (having a pure quadrupolar electric field), the cyclotron frequency is equal to the sum of the two radial frequencies: $\nu_c = \nu_+ + \nu_-$ [37].

Experimentally, the eigenmotions can be manipulated with different excitation techniques. The procedures for the two ISOLTRAP Penning traps are different since their functions are different. In the preparation trap, isobaric purification is achieved by applying a dipolar radio-frequency (rf) excitation with the mass-independent frequency ν_-, which leads to the increase of the magnetron radius of all ions (including contaminants) to a radius larger than that of the 1.5 mm trap exit hole. To select the ions of interest, a quadrupolar rf field with a frequency corresponding to ν_c of the ion of interest is applied to couple the two radial motions at the reduced cyclotron frequency ν_+ and magnetron frequency ν_-, resulting in a conversion from one to the other. Since ν_c is mass dependent, only for the ions of interest a full conversion of magnetron into cyclotron motion takes place. The cyclotron motion is damped due to collisions with the buffer gas, resulting in a centering of the resonantly excited ions which can then be ejected through the trap exit hole.

A second dipolar rf excitation can be applied at ν_+ of the contaminant ions, which leads to a quick increase in their cyclotron radius and collision with the trap electrodes. This allows a better cleaning when the contaminant is produced with much higher yield than the ion of interest. This technique was used, e.g., to remove the ^{66}Ga contaminant in the preparation Penning trap during the ^{66}Mn measurement.

In the precision Penning trap, first a dipolar rf excitation is applied at ν_- to increase the magnetron radius of the ions motion to about 0.7 mm. Then, a quadrupolar excitation near ν_c is applied before the extraction of the ions from the trap. If the excitation frequency reaches the resonant case $\nu_{RF} = \nu_c$ for a selected excitation time, a full conversion from the

magnetron to the cyclotron motion takes place. After ejection from the trap, the magnetic moments of the ions interact with the magnetic field gradient, producing an axial acceleration of the ions. At resonance, the magnetic moment and the associated radial kinetic energy reach their highest values, which results in the shortest time of flight (TOF) of the ions to the detector. A typical time-of-flight resonance curve and its analytical fit [31] are shown in the top left corner of Fig. 1.

III. RESULTS AND DISCUSSION

A. Data reduction and atomic mass evaluation

Each reported ISOLTRAP mass value m_{int} is based on the ratio of the measured frequency $\nu_{c,\text{int}}$ of the ion of interest and that of a reference ion $\nu_{c,\text{ref}}$ (with well known mass m_{ref}). The mass of interest can be deduced directly from this ratio:

$$m_{\text{int}} = \frac{\nu_{c,\text{ref}}}{\nu_{c,\text{int}}}(m_{\text{ref}} - m_{\text{e}}) + m_{\text{e}}, \quad (1)$$

where m_{e} is the electron mass.

In practice, Eq. (1) cannot be used directly since the reference mass is not an absolute atomic mass. In fact, each measurement represents a link between the reference ion and the ion of interest. Therefore, only the differences between atomic masses are measured and not the absolute atomic masses. Due to the large number of data available nowadays, one nuclide can have several links. To overcome the correlations in this complex network, the atomic mass evaluation (AME) is based on the least-square method weighted with the precision of each measurement or link. The AME gives relative atomic masses that can be adjusted each time a new link is given by measurement [38].

In this work, data from two separate experimental runs are combined. $^{39}K^{+}$ ions were used as a reference in the first experimental run for the $^{57-63}$Mn and $^{61-63}$Fe mass measurements. The Fe isotopes were not produced directly but were measured as decay products of the Mn isotopes in the Penning trap using the so-called in-trap decay method [39]. More technical details about the Fe isotope measurements will be given in an upcoming publication [40]. In the second experimental run $^{85}Rb^{+}$ ions were used as a reference for the $^{64-66}$Mn mass determinations. This region of the nuclear chart is very rich in isomeric states; however, no long-lived excited states are known and measured in any of the odd-A Mn isotopes. For two even-A Mn isotopes (^{58,60}Mn) only masses of the isomeric excited states were measured due to their long half-lives and their high production rate in comparison to the ground state. Due to their close masses, the ground-state and the isomeric state of ^{58}Mn were both present in the Penning trap during the measurement. However, due to the low production rate of the ground state, at least 5 times less than the excited isomeric state, the data analysis was restricted to less than 5 ions per cycle in order to eliminate any frequency shift related to the presence of the ground state. For ^{62}Mn only the mass of the longer-lived isomeric state was measured. Based on the high spin value of the first excited states of ^{58,60,64,66}Mn, we assumed that the measured high-spin isomer is the excited state.

For a mass determination the magnetic field strength is interpolated between measurements of the reference ion ($^{39}K^{+}$ or $^{85}Rb^{+}$) before and after each measurement of the ions of interest. The absence of shifts in the resonance frequency proportional to the number of trapped ions in all data indicates that no contamination was present [41]. Furthermore, the number of ions in the Penning trap was limited to 1–5 ions in order to eliminate any additional frequency shift that could be due to the ion-ion interaction. To account for unknown systematic effects a mass-independent systematic uncertainty of 8×10^{-9} is added. The treatment of the systematic uncertainties with the ISOLTRAP experimental setup is discussed in details in Ref. [30,41].

The accuracy of the experimental setup was tested using isotopes with well known masses. We measured $^{39}K^{+}$ using as reference $^{85}Rb^{+}$ for the first experimental run and $^{85}Rb^{+}$ using $^{133}Cs^{+}$ as reference for the second experimental run. None of the measurements showed a deviation from the tabulated masses, which indicates good stability of the experimental setup. Stable isotopes, ^{55}Mn and ^{48}Ti (produced at ISOLDE as titanium oxide TiO at mass $A = 64$), were used to test the stability as well. The resulting mass excess of ^{55}Mn is in good agreement with the tabulated value in AME2003 [38]. The ^{48}Ti mass excess determined from our stability test measurement shows a deviation from the tabulated mass in AME2003 but is in good agreement with recently published work by Faestermann *et al*. [42]. Our ^{48}Ti mass excess value contributed by 17% to the new tabulated mass and for both ^{48}Ti and ^{55}Mn; the mass precision was improved.

Table I shows the measured frequency ratios and the mass excess values resulting from the new atomic mass evaluation, which includes our results [43]. The latter are compared with values from the previous evaluation (AME2003) [38], and their contribution to the new mass values is presented. A clear improvement of the experimental uncertainties, mainly due to improved statistics, can be distinguished between the first and the second experimental runs. As an example, the statistical uncertainty of the ^{63}Mn frequency ratio was 8.1×10^{-8} in the first run while in the second run the ^{64}Mn statistical uncertainty was 4.4×10^{-8}. Unfortunately, due to the drop in the production yield of ^{66}Mn associated with the total transport efficiency and the decay loss due to the short half-life (64 ms), the uncertainty of ^{66}Mn is the largest. In Fig. 2 the new masses including the ISOLTRAP contributions are compared to data in AME2003 [38]. Almost all ISOLTRAP masses are more bound than the previously measured masses. $^{61-65}$Mn were determined by the Time-of-Flight Isochronous (TOFI) Spectrometer [44–46], using fragmented beams at high energies. This in-flight technique could easily have produced excited isomeric states that would not have been resolved by the spectrometer, which would result in less-bound masses. In the case of ^{58}Mn and ^{60}Mn, the ISOLTRAP values are less bound than the previously measured masses. These deviations could correspond to the excitation energies of the excited isomeric states within the uncertainties. Indeed, for ^{58}Mn we found that the mass value was not revised after the identification of the first excited isomeric state (see details in the ^{58}Mn discussion), which leads to a more bound ground state. However, we could not find the origin of ^{60}Mn mass value deviation from previous values and its link to the first isomeric states. The origin of the deviation of our ^{59}Mn mass value from

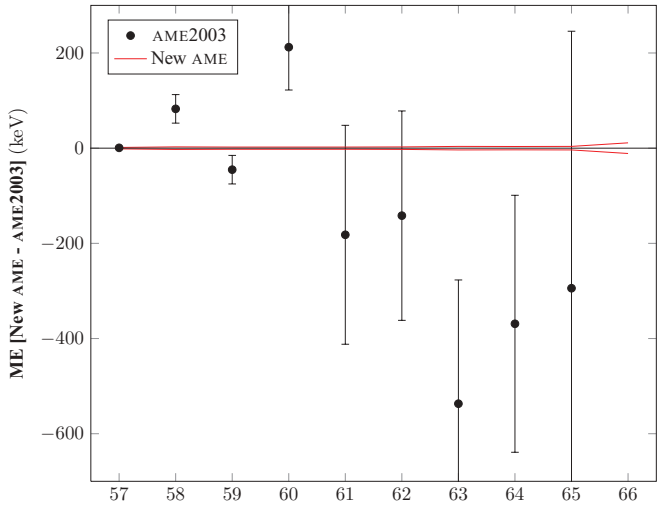

FIG. 2. (Color online) The new tabulated Mn mass excess values from Table I compared to the previously tabulated mass excesses from the atomic mass evaluation AME2003 [38]. The zero-line is the new data with their uncertainties represented by the red envelope, while the dots give the AME2003 values with their error bars.

the previous measurement (^{64}Ni(^{3}He,^{8}B)^{59}Mn reaction [47]) is also not clear. More details are given in the following paragraphs, where we discuss the mass measurements of the $^{57-66}$Mn and $^{61-63}$Fe isotopes individually.

^{57}Mn

Previously, the mass of ^{57}Mn has been measured in the ^{57}Mn(β^-)^{57}Fe decay giving a mass excess of −57486(50) keV [48]. It was also determined from a ^{54}Cr(α, p)^{57}Mn reaction [49,50], as well as a ^{55}Mn(t, p)^{57}Mn reaction [51] and ^{57}Cr(β^-)^{57}Mn β decay [52]. Recently, the mass of ^{57}Mn has been measured with ISOLTRAP [53] resulting in a mass excess of −57486.4(2.2) keV, which is in good agreement with the measurement presented in this work, −57484.1(2.6) keV. Due to their small uncertainties, the masses resulting from ISOLTRAP data and the reaction ^{55}Mn(t, p)^{57}Mn studied by Mateja *et al.* [51] [mass excess of −57485.1(3.6) keV] contribute as follows to the tabulated mass: 33% from this work (Table I), 49% from Guénaut *et al.* [53], and 17% from Mateja *et al.* [51].

^{58}Mn

We measured the frequency ratio of the long-lived isomeric state ^{58}Mn^{m+} to ^{39}K^{+}. From this ratio and the well known excitation energy of 71.78(5) keV, the mass of the ^{58}Mn ground state was extracted.

The decay of ^{58}Mn has been studied by Flynn *et al.* [54] using the reaction ^{58}Fe(t,^{3}He)^{58}Mn, in which 16 states (or groups) were observed. Since the peak width of the first state (group 0) is larger than the widths of the other states, they assumed that group "0" with $Q = -6318(15)$ keV was a mixture of the ground state and an excited isomeric state that they supposed to be located at 30(10) keV. The Q value measured in that experiment was corrected to

TABLE I. Frequency ratios from the ISOLTRAP measurements[a] and the resulting mass excesses (ME) after performing a new atomic mass evaluation. The contribution of ISOLTRAP to the new atomic mass value is shown in the last column as a percentage. The comparison between the new mass excess with the ISOLTRAP contribution and AME2003 [38] is plotted in Fig. 2.

Nuclide	Half-life [57]	ISOLTRAP frequency ratio	Reference ion	New AME ME (keV)	AME2003 ME (keV)	Contribution to new AME
^{48}Ti	Stable	0.753048782(13)[b]	^{85}Rb^{+}	−48491.7(0.4)	−48487.7(0.8)	10%
		1.163910127(22)[c]	^{55}Mn^{+}			7%
^{55}Mn	Stable	0.646999081(10)	^{85}Rb^{+}	−57711.6(0.5)	−57710.6(0.7)	36 %
		0.859172866(16)	TiO^{+}			21%
^{57}Mn	85.4(1.8) s	1.461322506(71)	^{39}K^{+}	−57486.1(1.5)	−57486.8(1.8)	33 %
^{58}Mn	3.0(1) s			−55827.4(2.7)	−55910(30)	
^{58}Mn^{m}	65.4(5) s	1.487035402(74)	^{39}K^{+}	−55755.6(2.7)	−55840(30)	100%
^{59}Mn	4.59(5) s	1.512707022(63)	^{39}K^{+}	−55525.2(2.3)	−55480(30)	100%
^{60}Mn	280(20) ms			−52967.8(2.3)	−53180(90)	
^{60}Mn^{m}	1.77(2) s	1.538450246(65)	^{39}K^{+}	−52695.9(2.3)	−52910(90)	100%
^{61}Mn	670(40) ms	1.564141801(65)	^{39}K^{+}	−51741.9(2.3)	−51560(230)	100%
^{61}Fe	5.98(6) min	1.563944015(73)	^{39}K^{+}	−58920.3(2.6)	−58921(20)	100%
^{62}Mn	92(13) ms				−48040(220)	
^{62}Mn^{m}	671(5) ms	1.589905194(72)	^{39}K^{+}	−48180.8(2.6)		100%
^{62}Fe	68(2) s	1.589610456(77)	^{39}K^{+}	−58877.9(2.8)	−58901(14)	100%
^{63}Mn	275(4) ms	1.615606112(102)	^{39}K^{+}	−46886.9(3.7)	−46350(260)	100%
^{63}Fe	6.1(6) s	1.615365034(155)	^{39}K^{+}	−55635.5(4.3)	−55550(170)	57%
^{64}Mn	90(4) ms	0.753178259(45)	^{85}Rb^{+}	−42989.0(3.5)	−42620(270)	100%
^{65}Mn	92(1) ms	0.764980824(48)	^{85}Rb^{+}	−40967.3(3.7)	−40670(540)	100%
^{66}Mn	65(2) ms	0.776811145(145)	^{85}Rb^{+}	−36750(11)		100%

[a] $^{57-63}$Mn and $^{61-63}$Fe isotopes were measured in the first experimental run with ^{39}K^{+} as the reference ion [40]. The other data were recorded in the second experimental run with ^{85}Rb^{+}, TiO^{+} and ^{55}Mn^{+} as reference ions.

[b] This is the frequency ratio of TiO^{+} to ^{85}Rb^{+}.

[c] This is the frequency ratio of TiO^{+} to ^{55}Mn^{+}.

$Q = -6300(30)$ keV giving a ground-state mass excess of $-55832(30)$ keV. Later, Schmidt-Ott *et al.* [55] discovered the excited isomeric state at 71.78(5) keV with 68(9) s half-life. It was then assumed, in AME1993 [56] as well as in AME2003 [38], that the lower state observed by Flynn *et al.* was the long-lived isomer. The deduced ground-state mass excess was thus $-55900(30)$ keV in AME1993 and $-55910(30)$ keV in AME2003. Reexamining the paper of Flynn *et al.* [54] in light of the most recent Evaluated Nuclear Structure Data File (ENSDF) [57], we found that the first excited state, group 1, at 77(8) keV identified by Flynn *et al.* is precisely the excited isomeric state in ENSDF at 71.78(5) keV. This means that the group 0 in Ref. [54] was not a mixture but a pure ground state. Their original Q value should not have been corrected and the mass excess of the ground state should thus be $-55817(15)$ keV, which agrees with the ISOLTRAP value $-55827.4(2.7)$ keV within quoted uncertainties. The new adjusted $(t,^3\mathrm{He})$ energy $-6308.1(2.8)$ keV is in very good agreement with Flynn's original result. The very first measurements of the ^{58}Mn mass were performed in the late 1960s from β-decay energy measurements [58,59] with a total Q_β of, respectively, 5890(100) and 5958(100) keV. Our measurement combined with the ^{58}Fe mass results in a Q_β of 6326.8(2.8) keV. As is often the case with high-energy Q_β measurements [60], the previously measured Q_β are strongly underestimated. The ISOLTRAP value for the mass of ^{58}Mn is now the sole input to the new AME, due to its small uncertainty.

^{59}Mn

The mass of ^{59}Mn was measured by Kashy *et al.* [47] using the reaction ^{64}Ni(^{3}He,^{8}B)^{59}Mn and by Pardo *et al.* [61] at Argonne National Laboratory from β decay. Only the ^{64}Ni(^{3}He,^{8}B)^{59}Mn reaction energy of $-19610(30)$ keV was used in AME2003, which combined with the most recent mass value of ^{64}Ni, resulted in a mass excess of $-55480(30)$ keV. Our result yields a corresponding reaction energy of $-19563.4(2.6)$ keV, moving the Kashy *et al.* result 1.6σ from ours. The β-decay result from Pardo *et al.* of 5200(100) keV agrees with our result of 5140(3) keV. Due to its small uncertainty, the ISOLTRAP mass excess value of $-55525.2(2.3)$ keV is now used as the only input for the mass of ^{59}Mn.

^{60}Mn

The frequency ratio between the long-lived isomer $^{60}\mathrm{Mn}^{m+}$ and $^{39}\mathrm{K}^{+}$ was measured. The known isomeric energy is 271.9(1) keV. By using a long excitation duration in our Penning trap it was possible to resolve the ground and the excited states. The ground state, having a shorter half-life, decayed away during the 1.2-s excitation time.

The decay of ^{60}Mn has been studied by Norman *et al.* [62]. The half-life was reported to be 1.79(10) s and 3^+ was proposed to be the ground state's spin and parity. The Q_β value was measured to be 8510(100) keV, which corresponds to a mass excess of $-52890(100)$ keV. Later, this 3^+ level was shown to be an excited isomeric state [63]. The first measurement of the presumed 0^+ ground state's half-life of 51(6) s was achieved by Bosch *et al.* [64]. Recently, the half-life of the ^{60}Mn ground state has been measured to be 0.28(2) s [65], while spins and parities 1^+ and 4^+ were assigned to the ground and excited isomeric states, respectively. The Q_β value was corrected and a mass excess of $-53178(90)$ keV was deduced. Our measurement yields a mass excess of $-52967.8(2.3)$ keV and a Q_β of 8445(4) keV. The previously measured and corrected mass is 2σ away from our value.

The ^{60}Mn mass was also measured by the TOFI instrument at Los Alamos [44–46], yielding mass excesses of $-52540(230)$, $-52780(260)$, and $-52520(250)$ keV, respectively. Our mass excess value does not agree with these measurements except for the second measurement. Due to its small uncertainty, the ISOLTRAP value is taken as the new tabulated mass.

^{61}Mn

Previously, the mass of ^{61}Mn was measured in three experiments by the TOFI group at Los Alamos [44–46], with the average giving the mass excess value of $-51560(230)$ keV. The ISOLTRAP measurement yields a value of $-51741.9(2.3)$ keV, in agreement with the previous value but two orders of magnitude more precise. Therefore, our value is taken as the sole input to the new AME.

^{61}Fe

The mass of ^{61}Fe was deduced from the ^{64}Ni(α,^{7}Be)^{61}Fe reaction [66]. The mass excess is $-58920(20)$ keV, in good agreement with our value of $-58920.3(2.6)$ keV. Our result is eight times more precise and determines the mass of ^{61}Fe to 100%. The Q_β value for ^{61}Fe was measured earlier and gave values of 3827(100) keV [67] and 3887(100) keV [68]. Our result gives a Q_β value of 3977.1(2.8) keV, which agrees with both values.

The ^{61}Fe mass was also determined from the ^{62}Ni(^{14}C,^{15}O)^{61}Fe reaction [69] and gave a value of $-7921(100)$ keV, 2.6σ away from our equivalent value of $-7661.1(2.7)$ keV. Another reaction, ^{64}Ni(^{14}C,^{17}O)^{61}Fe, cited as private communication from Bernas *et al.* in Ref. [69], gave a value of $-4609(100)$ keV. This value is also 2.6σ away from our equivalent value of $-4349.3(2.7)$ keV. The excited isomeric state of ^{61}Fe has a half-life of 250(10) ns, too short to be measured in our trap.

^{62}Mn

Only the mass of the long-lived [671(5) ms] high-spin isomer [21] was measured for ^{62}Mn. The short-lived isomer [92(13) ms] was highly suppressed due to low production and long experimental cycle; no significant ion number of the short-lived isomer was left in the Penning trap during the measurement. Until now it was not known which one of these two isomers is the ground state. The high spin is assigned to the excited longer-lived isomeric state. As stated above, based on the high-spin value of the first excited states of ^{58,60,64,66}Mn, we assumed here that the measured mass is that of the excited isomeric state since it is assigned to high spin.

The previous ^{62}Mn mass excess (in AME2003) of $-48040(220)$ keV was the average value from three experiments by the TOFI group [44–46]. Our mass excess value is $-48180.8(2.6)$ keV and agrees with the average of the previous measurements but with two orders of magnitude reduced uncertainty. Our value is thus taken as the sole input to the new AME.

^{62}Fe

The mass of ^{62}Fe was measured in several heavy-ion reaction experiments on ^{64}Ni but only four of them were used

to calculate the average of the mass excess given in AME2003, of −58901(14) keV [70–73]. The ISOLTRAP value of −58877.9(2.8) keV agrees with all these except with Ref. [72], which is 2σ away. Earlier, a β-decay measurement [74] gave a Q_β of 3000(200) keV, 2.2σ away from our result of 2553(20) keV. Due to its high precision, ISOLTRAP carries 100% significance in the determination of the ^{62}Fe mass in the new AME.

^{63}Mn

The mass of ^{63}Mn was previously measured in three different experiments with TOFI [44–46], giving an average mass excess value of −46350(260) keV. This value is 2σ away from our measured mass excess of −46886.9(3.7) keV. More recently, the mass was measured by Knöbel at GSI-ESR [75], also with a TOF method, yielding a mass excess of −47347(95) keV. This value deviates from the ISOLTRAP measurement by 4.8 σ. Due to its small uncertainty, the ISOLTRAP mass excess is taken as the final value in the new AME.

^{63}Fe

The mass excess of ^{63}Fe was measured in three TOFI experiments [44–46] with an average value of −55550(170) keV. The ISOLTRAP measurement gives a mass excess of −55636.6(5.7) keV, which is in a good agreement with the TOFI experiments. This is also in good agreement with the recent LEBIT value [19] −55634.1(6.7) keV. The final mass excess of −55635.5(4.3) keV is the weighted average of both Penning trap measurements.

^{64}Mn

The mass of ^{64}Mn was also given by the average of three TOFI measurements [44–46], resulting in a mass excess of −42620(270) keV. The ISOLTRAP measurement gives a value of −42989.0(3.5) keV, within 1.4 σ of the average value of these measurements.

The excited isomer is not present in the ISOLTRAP measurement because of its short half-life of 500(50) μs [76].

Due to its small uncertainty, the ISOLTRAP mass value is taken as the sole input to the new AME.

^{65}Mn

The mass of ^{65}Mn was given in AME2003 as the average of two TOFI measurements; the average mass excess was reported to be −40670(540) keV [45,46]. This compares to the ISOLTRAP measurement of −40967.3(3.7) keV, which is in good agreement. Our result agrees also with the recent time-of-flight measurement by Estradé *et al.* [77] that gave a mass excess value of −40790(310) keV. Due to the large uncertainties of the previous measurements, the ISOLTRAP value is taken as the new tabulated mass excess.

^{66}Mn

Recently the mass of ^{66}Mn was determined with mass excess of −36900(790) keV [77]. The ISOLTRAP measurement gives a ground state mass excess of −36750.4(11.2) keV, which is in good agreement with the recent measurement. Due to its small uncertainty the ISOLTRAP mass is taken to determine the mass of ^{66}Mn.

The half-life of this nuclide of 65(2) ms makes it the one with the shortest half-life ever studied with ISOLTRAP. The isomeric state measured recently [76] with a half-life of 750(250) μs is not present in our measurement.

B. The new mass surface

1. The two-neutron separation energy

The two-neutron separation energy

$$S_{2n}(N, Z) = B(N, Z) - B(N - 2, Z), \tag{2}$$

where $B(N, Z)$ is the binding energy of the nucleus with proton number Z and neutron number N, is a remarkable quantity in which shell structure manifests itself. The two-neutron separation energy generally decreases smoothly with increasing N, reflecting the shell filling. A sudden drop of the S_{2n} values indicates a shell closure (or magic number) since less energy is required to remove a pair of neutrons outside the closed shell. In Fig. 3, the new S_{2n} values are plotted between the neutron numbers $N = 30$ and $N = 52$. At the well known closed shell $N = 50$ a sudden drop is visible; however, no such drop is visible at $N = 40$ for the Mn isotopic chain. In the isotopic chains $Z = 32$–36 (Ge–Kr), the expected linear trend is observed. Starting from the Ga isotopic chain, irregularities in the mass surface appear. Recent nuclear spin and magnetic moment measurements of Cu and Ga isotopes [78–82] reveal a sudden change in structure in this region. These effects are enhanced for lighter nuclides, and for the Mn isotopic chain one can see a significant increase in S_{2n} values at $N = 38$ due to gain in binding energy, which could be interpreted as a result of strong deformation.

Note the behavior of the ^{66}Mn S_{2n} value, which is very close to ^{65}Mn S_{2n} value. For the ^{64,65}Mn isotopes the S_{2n}-value decrease is much larger.

2. The empirical shell gap

The shell gap is defined as the energy difference between shells in the single-particle shell model. In the case of $N = 40$ this would be the distance between the pf shell and the g shell.

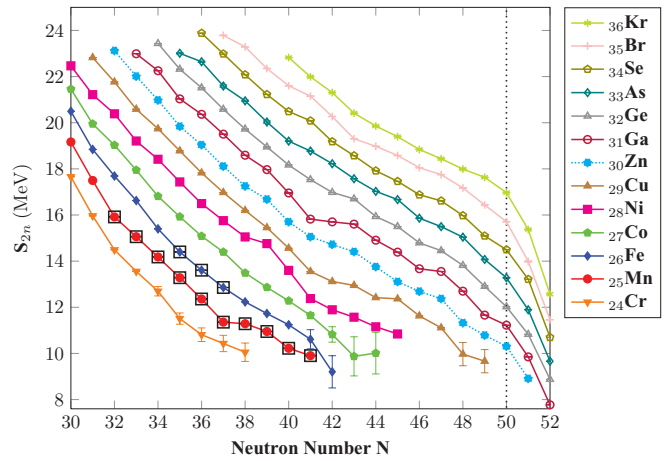

FIG. 3. (Color online) The two-neutron separation energy S_{2n} plotted for neutron numbers $N = 30$–52 from Cr ($Z = 24$) to Kr isotopes ($Z = 36$). The squares mark the isotopes measured in this work along the Mn and Fe isotopic chains.

The experimentally accessible "empirical shell gap" [83]

$$\Delta_N(N, Z) = S_{2n}(N, Z) - S_{2n}(N + 2, Z), \tag{3}$$

in addition to the single particle shell gap, includes many-body effects. This second mass derivative quantifies in a simple way the strength of the shell closure. In the case of the well established magic numbers, the empirical shell gap can reach several MeV. For the doubly-magic nuclides $^{32}_{16}S_{16}$ and $^{56}_{28}Ni_{28}$, it even reaches 8 MeV. This quantity varies between 1 and 2 MeV for $N = 40$.

The empirical shell gap can be visualized from the spacing between $-S_{2n}/2$ for $N = 40$ and $N = 42$ for different Z. This spacing can be better seen by subtracting the same linear trend, $F(Z)$, from the $-S_{2n}/2$ values as shown in Fig. 4. The slope of $F(Z)$ was obtained by fitting the experimental $-S_{2n}/2$ values between $Z = 26$ and $Z = 38$, taken from the new AME [43]. The energy difference between $N = 40$ and $N = 42$ increases when approaching $Z = 28$ and $Z = 40$ and is very small in between. This gap has a maximum value below 1 MeV which is still very small compared to the gap at $N = 50$ and $N = 52$ (2–4 MeV, shown in Fig. 2 of Ref. [84]). Hence, the empirical shell gap is clearly too small to consider $N = 40$ as a magic number.

Figure 4 shows also the theoretical predictions of the S_{2n} values using the spherical mean field and the deformed model with the angular-momentum projected general coordinate method [84]. The significant reduction of the spherical shell gap, when the correlations are included by the angular-momentum projected GCM, is in relatively good agreement with the experimental data. While the scale of this effect is nicely reproduced in the mean-field calculations, it is clear that this approach cannot yet predict the fine structure. Moreover, these state-of-the-art calculations are still only available for even-even nuclides. It is also worth noting that the mean-field Gogny calculations of Gaudefroy *et al.* [12] and the state-of-the-art shell model calculations by Lenzi *et al.* [11] around $N = 40$ are likewise only performed for even-even nuclides.

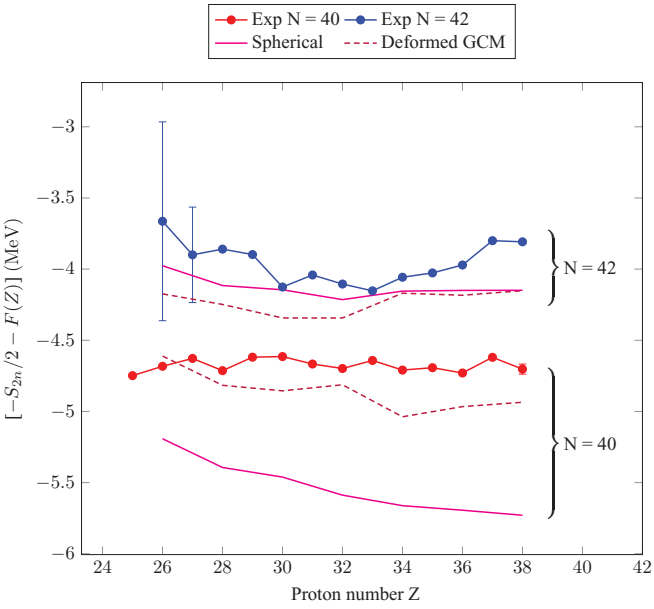

FIG. 4. (Color online) The two-neutron separation energy with subtraction of a linear trend $F(Z)$ plotted as a function of the proton number for the chains of isotones with $N = 40$ and $N = 42$; all data are taken from the new AME [43]. The distance between the $N = 40$ and $N = 42$ curves corresponds to the empirical shell gap. Solid lines correspond to calculated values from spherical mean field and the dashed ones are calculated using the general coordinate method of $J = 0$ projected axial quadrupole ($J = 0$ GCM) [84] (only available for even-even nuclei).

3. *The pairing gap and the proton-neutron interaction*

In order to understand the deformation indicated by the two-neutron separation energies of the Mn isotopes at $N = 38$ and beyond (see Fig. 3), we tried to extract the strength of the "empirical proton-neutron interaction," as it is known, to drive nuclei to deformation. Extracting the proton-neutron interaction strength from experimental binding energies is not always reliable since the latter contain the sum of all interactions inside the nucleus [85,86]. However, we believe that if one of the interactions is dominant, its influence should be seen in the mass derivatives, as is the case for the shell closure in the two-neutron separation energies. To approximate the strength of the proton-neutron interaction we choose the difference in pairing gaps of Z-even and Z-odd nuclei [87–89]. This definition allows us to track both the pairing interaction and proton-neutron interaction from the same figure, which is suited for this case where there is a clear competition between these two interactions.

The neutron pairing gap can be approximated as

$$P_n(Z, N) = \frac{(-1)^{N+1}}{4}[S_n(Z, N + 1) - 2S_n(Z, N) + S_n(Z, N - 1)] \tag{4}$$

$$= \frac{(-1)^{N+1}}{4}[B(Z, N + 1) - 3B(Z, N) + 3B(Z, N - 1) - B(Z, N - 2)], \tag{5}$$

where S_n is the neutron separation energy and B is the binding energy.

The neutron pairing for odd-Z nuclei is smaller than for even-Z nuclei. This difference can be due to the proton-neutron interaction between the last unpaired proton and neutron [87–89]. Thus, we can define the empirical proton-neutron interaction as being the difference between odd- and even-Z neutron pairing gap:

$$\Delta_{np} = (-1)^Z[P_n(N, Z) - P_n(N, Z - 1)]. \tag{6}$$

Graphically, Δ_{np} is the distance between the neutron pairing curve for Z and $Z - 1$. Figure 5 shows the experimental values of the neutron pairing gap P_n calculated from the new tabulated masses of Mn isotopes ($Z = 25$) and their neighboring Fe isotopes ($Z = 26$) [43]. At a closed shell the neutron pairing gap P_n should increase suddenly, indicating the large energy needed to break a neutron pair and promote one of the neutrons to a new shell. From the new Mn neutron-pairing gap values, such an effect is not visible, which confirms the previous conclusion that the $N = 40$ is not a shell closure.

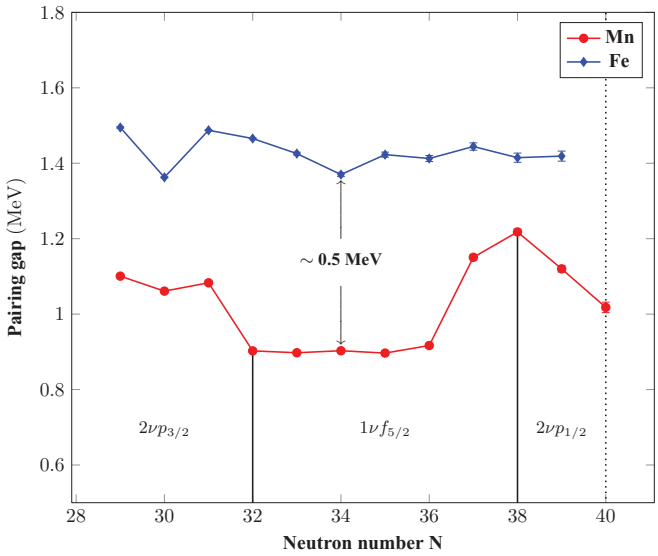

FIG. 5. (Color online) The experimental neutron pairing gaps plotted as a function of the neutron number for the Mn isotopes ($Z = 25$) and Fe isotopes ($Z = 26$). These pairing gaps are calculated from the new AME [43]. The single-particle shell model levels (as expected in the spherical nuclei) are shown for the neutrons. The proton-neutron interaction could be estimated to be around 0.5 MeV from the distance between the pairing curves of the even-Z isotopes (Fe) and the odd-Z isotopes (Mn). Note that the error bars are smaller than the data points.

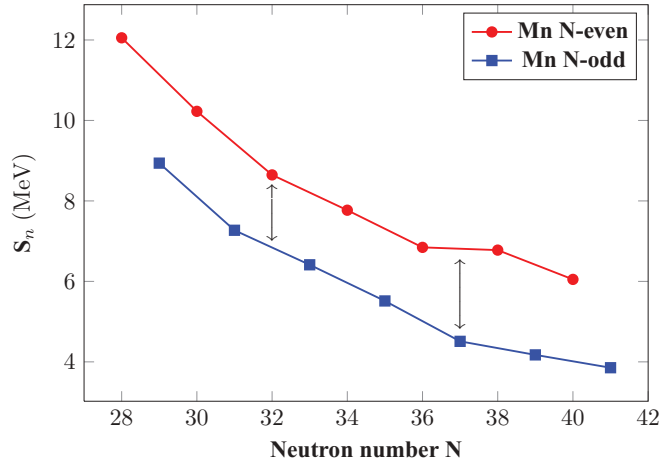

FIG. 6. (Color online) The neutron separation energy (S_n) values for Mn isotopes as a function of the neutron number [43]. The neutron pairing gap is the distance between the odd-N and even-N curves. One can see the increase of the pairing at $N = 37$ caused by the increase of the S_n values at $N = 38$.

The pairing gap of the Mn isotopes drops at $N = 32$ and increases at $N = 37$. The drop at $N = 32$ could correspond to the neutron filling of the $1\nu f_{5/2}$ orbital in the spherical shell model. If the protons and neutrons are in the same shell ($1\pi f_{7/2}$, $1\nu f_{5/2}$) the proton-neutron interaction should increase, inducing a lowering of the $1\nu f_{5/2}$ orbital. This increase results in lower pairing gaps for the odd-Z nuclides [see Eq. (6)], which takes place at $N = 32$ as shown in Fig. 5. In a first assumption we can estimate this proton-neutron interaction from the distance between the two curves to be around 0.5 MeV. A large increase in the pairing energies at $N = 37$ can be seen from Fig. 5. Examining the Mn neutron separation S_n values plotted versus the neutron number N in Fig. 6, the distance between the odd-N and even-N Mn S_n curves from $N = 32$ to $N = 36$ is constant [by definition this distance is the pairing gap in Eq. (4)]. At $N = 37$ this distance is larger because of the increase in the neutron separation energy at $N = 38$. A possible explanation for this change of slope is that neutrons start to occupy higher shells already at $N = 38$. This interpretation is in good agreement with the observed long half-lives of the Mn isotopes, which could not be reproduced in theory without the g shell [24]. At $N = 38$, the neutron–proton ratio is large enough that the pairing effect overshadows the proton-neutron interaction [15,24,28,29].

No firm conclusion can be made from the pairing gap concerning the occupation of the single-particle orbitals because of the collective effects which cannot be disentangled from the total binding energy. Recent theoretical calculations in this region showed that the neutron configuration is very complex. The enhancement of collectivity observed in the Fe and Cr neutron-rich isotopes [9,16] has been found to be due to the occupation of the $1\nu g_{9/2}$ intruder state and even the $2\nu d_{5/2}$ orbital. The calculations using a larger valence space showed that the many-particle many-hole configuration seems to predominate in the wave functions of the deformed ground states [11]. Furthermore, the region below neutron-rich Ni was recently compared to the island of inversion around the neutron-rich Mg isotopes [8,9,11]. The $N = 20$ gap or the spacing between the single particle $2\nu d_{3/2}$–$1\nu f_{7/2}$ is reduced when protons are removed from the $1\pi d_{5/2}$ orbital. In both regions, the neutron quadrupole partner orbitals are responsible for the observed deformation. However, unlike $N = 20$, $N = 40$ is not a classical magic number and the analogy between the two regions might be questionable, as stressed in Ref. [9].

The mechanism responsible for the deformation of the neutron-rich Mn isotopes may then be considered as the same as that responsible for the deformation observed in the island of inversion around $N = 20$ (i.e., promotion of neutron pairs to higher orbitals).

IV. SUMMARY

High-precision mass measurements of the neutron-rich manganese and iron isotopes ($^{57-66}$Mn and $^{61-63}$Fe) have been performed with the ISOLTRAP mass spectrometer. The new mass surface showed no evidence for a shell closure at $N = 40$ for the Mn isotopes. However, the two-neutron separation energy showed a sudden increase at $N = 38$. Recent β-decay and spectroscopy measurements revealed an increase of collectivity due to deformations arising in this region, which is in good agreement with the new measured masses. These deformations may find their origin in the neutron occupation of a higher shell, with the $1\nu g_{9/2}$ and $2\nu d_{5/2}$ orbitals. The occupation of these intruder states is probably due to the weakening of the proton-neutron interaction when protons are removed from $1\pi f_{7/2}$ orbital. The strength of

the empirical proton-neutron interaction can be approximated from the new binding energies to be around 0.5 MeV. At $N = 38$, the neutron pairing predominates, which is consistent with the statement that neutron pairs scatter to a higher shell.

Our results support the collectivity observed around $N = 40$ and the similarity between this region and the island of inversion around $N = 20$. The Mn isotopes starting from ^{63}Mn are most likely within this new island of inversion.

ACKNOWLEDGMENTS

This work was supported by the German Federal Ministry for Education and Research (BMBF) (Grants No. 06GF9102, No. 06MZ215, and No. 06DD9054), the French IN2P3, the Max-Planck Society and the Japan Society for the Promotion of Science. We are grateful to the members of the ISOLDE technical group and the ISOLDE Collaboration for their support.

[1] C. Thibault, R. Klapisch, C. Rigaud, A. M. Poskanzer, R. Prieels, L. Lessard, and W. Reisdorf, Phys. Rev. C **12**, 644 (1975).
[2] C. Détraz, D. Guillemaud, G. Huber, R. Klapisch, M. Langevin, F. Naulin, C. Thibault, L. C. Carraz, and F. Touchard, Phys. Rev. C **19**, 164 (1979).
[3] X. Campi, H. Flocard, A. K. Kerman, and S. Koonin, Nucl. Phys. A **251**, 193 (1975).
[4] E. K. Warburton, J. A. Becker, and B. A. Brown, Phys. Rev. C **41**, 1147 (1990).
[5] G. Neyens, M. Kowalska, D. Yordanov, K. Blaum, P. Himpe, P. Lievens, S. Mallion, R. Neugart, N. Vermeulen, Y. Utsuno, and T. Otsuka, Phys. Rev. Lett. **94**, 022501 (2005).
[6] M. Kowalska, D. T. Yordanov, K. Blaum, P. Himpe, P. Lievens, S. Mallion, R. Neugart, G. Neyens, and N. Vermeulen, Phys. Rev. C **77**, 034307 (2008).
[7] K. Wimmer *et al.*, Phys. Rev. Lett. **105**, 252501 (2010).
[8] P. Adrich, A. M. Amthor, D. Bazin, M. D. Bowen, B. A. Brown, C. M. Campbell, J. M. Cook, A. Gade, D. Galaviz, T. Glasmacher, S. McDaniel, D. Miller, A. Obertelli, Y. Shimbara, K. P. Siwek, J. A. Tostevin, and D. Weisshaar, Phys. Rev. C **77**, 054306 (2008).
[9] J. Ljungvall *et al.*, Phys. Rev. C **81**, 061301(R) (2010).
[10] D. Pauwels, O. Ivanov, N. Bree, J. Büscher, T. E. Cocolios, J. Gentens, M. Huyse, A. Korgul, Yu. Kudryavtsev, R. Raabe, M. Sawicka, I. Stefanescu, J. Van de Walle, P. Van den Bergh, P. Van Duppen, and W. B. Walters, Phys. Rev. C **78**, 041307(R) (2008).
[11] S. M. Lenzi, F. Nowacki, A. Poves, and K. Sieja, Phys. Rev. C **82**, 054301 (2010).
[12] L. Gaudefroy, A. Obertelli, S. Péru, N. Pillet, S. Hilaire, J.-P. Delaroche, M. Girod, and J. Libert, Phys. Rev. C **80**, 064313 (2009).
[13] M. Bernas, Ph. Dessagne, M. Langevin, J. Payet, F. Pougheon, and P. Roussel, Phys. Lett. B **113**, 279 (1982).
[14] R. Broda, B. Fornal, W. Królas, T. Pawłat, D. Bazzacco, S. Lunardi, C. Rossi-Alvarez, R. Menegazzo, G. de Angelis, P. Bednarczyk, J. Rico, D. De Acuña, P. J. Daly, R. H. Mayer, M. Sferrazza, H. Grawe, K. H. Maier, and R. Schubart, Phys. Rev. Lett. **74**, 868 (1995).
[15] O. Sorlin *et al.*, Phys. Rev. Lett. **88**, 092501 (2002).
[16] A. Gade *et al.*, Phys. Rev. C **81**, 051304(R) (2010).
[17] W. Rother *et al.*, Phys. Rev. Lett. **106**, 022502 (2011).
[18] C. Guénaut, G. Audi, D. Beck, K. Blaum, G. Bollen, P. Delahaye, F. Herfurth, A. Kellerbauer, H.-J. Kluge, J. Libert, D. Lunney, S. Schwarz, L. Schweikhard, and C. Yazidjian, Phys. Rev. C **75**, 044303 (2007).
[19] R. Ferrer, M. Block, C. Bachelet, B. R. Barquest, G. Bollen, C. M. Campbell, M. Facina, C. M. Folden, C. Guénaut, A. A. Kwiatkowski, D. L. Lincoln, D. J. Morrissey, G. K. Pang, A. M. Prinke, R. Ringle, J. Savory, P. Schury, and S. Schwarz, Phys. Rev. C **81**, 044318 (2010).
[20] M. Bernas, P. Armbruster, S. Czajkowski, H. Faust, J. P. Bocquet, and R. Brissot, Phys. Rev. Lett. **67**, 3661 (1991).
[21] M. Hannawald, T. Kautzsch, A. Wöhr, W. B. Walters, K.-L. Kratz, V. N. Fedoseyev, V. I. Mishin, W. Böhmer, B. Pfeiffer, V. Sebastian, Y. Jading, U. Köster, J. Lettry, and H. L. Ravn (the ISOLDE Collaboration), Phys. Rev. Lett. **82**, 1391 (1999).
[22] O. Sorlin *et al.*, Nucl. Phys. A **660**, 3 (1999).
[23] O. Sorlin *et al.*, Nucl. Phys. A **719**, 193c (2003).
[24] L. Gaudefroy *et al.*, Eur. Phys. J. A **23**, 41 (2005).
[25] D. Pauwels *et al.*, Phys. Rev. C **79**, 044309 (2009).
[26] J. M. Daugas *et al.*, Phys. Rev. C **83**, 054312 (2011).
[27] R. Grzywacz *et al.*, Phys. Rev. Lett. **81**, 766 (1998).
[28] O. Sorlin *et al.*, Eur. Phys. J. A **16**, 55 (2003).
[29] H. Grawe, M. Górska, J. Döring, C. Fahlander, M. Palacz, F. Nowacki, E. Caurier, J. M. Daugas, M. Lewitowicz, M. Sawicka, M. Pfiitzner, R. Grzywacz, K. Rykaczewski, O. Sorlin, S. Leenhardt, F. Azaiez, M. Rejmund, K. Hauschild, and J. Uusitalo, in *Tours Symposium on Nuclear Physics IV, Tours 2000*, AIP Conf. Proc. 561 (AIP, New York, 2001), p. 287.
[30] M. Mukherjee, D. Beck, K. Blaum, G. Bollen, J. Dilling, S. George, F. Herfurth, A. Herlert, A. Kellerbauer, H.-J. Kluge, S. Schwarz, L. Schweikhard, and C. Yazidjian, Eur. Phys. J. A **35**, 1 (2008).
[31] M. König, G. Bollen, H.-J. Kluge, T. Otto, and J. Szerypo, Int. J. Mass Spectrom. Ion Processes **142**, 95 (1995).
[32] E. Kugler, Hyperfine Interact. **129**, 23 (2000).
[33] H. J. Kluge, F. Ames, W. Ruster, and K. Wallmeroth, *Proceedings of the Accelerated Beams Workshop, Parksville*, edited by L. Buchmann and J. M. D'Auria, TRIUMPF Report No. TRI-851, 1985, p. 119.
[34] U. Köster, Nucl. Phys. A **701**, 441c (2002).
[35] F. Herfurth, J. Dilling, A. Kellerbauer, G. Bollen, S. Henry, H.-J. Kluge, E. Lamour, D. Lunney, R. B. Moore, C. Scheidenberger, S. Schwarz, G. Sikler, and J. Szerypo, Nucl. Instrum. Methods Phys. Res., Sect. A **469**, 254 (2001).
[36] G. Savard, St. Becker, G. Bollen, H.-J. Kluge, R. B. Moore, Th. Otto, L. Schweikhard, H. Stolzenberg, and U. Wiess, Phys. Lett. A **158**, 247 (1991).
[37] L. S. Brown and G. Gabrielse, Rev. Mod. Phys. **58**, 233 (1986).
[38] G. Audi, A. H. Wapstra, and C. Thibault, Nucl. Phys. A **729**, 337 (2003).

[39] A. Herlert, D. Beck, K. Blaum, F. Carrel, P. Delahaye, S. George, C. Guénaut, F. Herfurth, A. Kellerbauer, H.-J. Kluge, D. Lunney, M. Mukherjee, L. Schweikhard, and C. Yazidjian, New J. Phys. **7**, 44 (2005).

[40] A. Herlert, S. Van Gorp, D. Beck, K. Blaum, M. Breitenfeldt, R. B. Cakirli, S. George, U. Hager, F. Herfurth, A. Kellerbauer, D. Lunney, R. Savreux, L. Schweikhard, and C. Yazidjian (accepted in Eur. Phys. J. A.).

[41] A. Kellerbauer, K. Blaum, G. Bollen, F. Herfurth, H.-J. Kluge, M. Kuckein, E. Sauvan, C. Scheidenberger, and L. Schweikhard, Eur. Phys. J. D **22**, 53 (2003).

[42] T. Faestermann, R. Hertenberger, H.-F. Wirth, R. Krücken, M. Mahgoub, and P. Maier-Komor, Eur. Phys. J. A **42**, 339 (2009).

[43] The Atomic Mass Evaluation, 2011, [http://amdc.in2p3.fr/masstables/Ame2011int/filel.html].

[44] X. L. Tu, X. G. Zhou, D. J. Vieira, J. M. Wouters, Z. Y. Zhou, H. L. Seifert, and V. G. Lind, Z. Phys. A **337**, 361 (1990).

[45] H. L. Seifert, J. M. Wouters, D. J. Vieira, H. Wollnik, X. G. Zhou, X. L. Tu, Z. Y. Zhou, and G. W. Butler, Z. Phys. A **349**, 25 (1994).

[46] Y. Bai, D. J. Vieira, H. L. Seifert, and J. M. Wouters (private communication).

[47] E. Kashy, W. Benenson, D. Mueller, H. Nann, and L. Robinson, Phys. Rev. C **14**, 1773 (1976).

[48] S. S. Vasilev and L. Y. Shavtvalov, Zh. Eskp. Teor. Fiz. **45**, 1385 (1963).

[49] J. F. Mateja, G. F. Neal, J. D. Goss, P. R. Chagnon, and C. P. Browne, Phys. Rev. C **13**, 118 (1976).

[50] K. A. Aniol, D. W. Gebbie, C. L. Hollas, and J. Nurzynski, Nucl. Phys. A **303**, 154 (1978).

[51] J. F. Mateja, C. P. Browne, C. E. Moss, and J. B. McGrory, Phys. Rev. C **15**, 1708 (1977).

[52] C. N. Davids, D. F. Geesaman, S. L. Tabor, M. J. Murphy, E. B. Norman, and R. C. Pardo, Phys. Rev. C **17**, 1815 (1978).

[53] C. Guénaut, G. Audi, D. Beck, K. Blaum, G. Bollen, P. Delahaye, F. Herfurth, A. Kellerbauer, H.-J. Kluge, D. Lunney, S. Schwarz, L. Schweikhard, and C. Yazidjian, Eur. Phys. J. A. **25**, 35 (2005).

[54] E. R. Flynn, J. W. Sunier, and F. Ajzenberg-Selove, Phys. Rev. C **15**, 879 (1977).

[55] W.-D. Schmidt-Ott, K. Becker, U. Bosch-Wicke, T. Hild, F. Meissner, R. Kirchner, E. Roeckl, and K. Rykaczewski, in *Proceedings 6th International Conference on Nuclei Far from Stability and 9th International Conference on Atomic Masses and Fundamental Constants, Bernkastel-Kues, Germany*, edited by R. Neugart and A. Wohr (Institute of Physics (IOP), Bristol, 1993), p. 627.

[56] G. Audi and A. H. Wapstra, Nucl. Phys. A **565**, 1 (1993).

[57] Evaluated Nuclear Structure Data File, 2010, [http://www.nndc.bnl.gov/ensdf/].

[58] T. E. Ward, P. H. Pile, and P. K. Kuroda, Phys. Rev. **182**, 1186 (1969).

[59] N. C. Dyer and J. H. Hamilton, Nucl. Phys. A **173**, 393 (1971).

[60] G. Audi, M. Wang, A. H. Wapstra, B. Pfeiffer, and F. C. Kondev, J. Korean Phys. Soc. **59**, 1318 (2011).

[61] R. C. Pardo, C. N. Davids, M. J. Murphy, E. B. Norman, and L. A. Parks, Phys. Rev. C **16**, 370 (1977).

[62] E. B. Norman, C. N. Davids, M. J. Murphy, and R. C. Pardo, Phys. Rev. C **17**, 2176 (1978).

[63] E. Runte, K.-L. Gippert, W.-D. Schmidt-Ott, P. Tidemand-Petersson, L. Ziegeler, R. Kirchner, O. Klepper, P. O. Larsson, E. Roeckl, D. Schardt, N. Kaffrell, P. Peuser, M. Bernas, P. Dessagne, M. Langevin, and K. Rykaczewski, Nucl. Phys. A **441**, 237 (1985).

[64] U. Bosch, W.-D. Schmidt-Ott, E. Runte, P. Tidemand-Petersson, P. Koschel, F. Meissner, R. Kirchner, O. Klepper, E. Roeckl, K. Rykaczewski, and D. Schardt, Nucl. Phys. A **477**, 89 (1988).

[65] S. N. Liddick, P. F. Mantica, B. A. Brown, M. P. Carpenter, A. D. Davies, M. Horoi, R. V. F. Janssens, A. C. Morton, W. F. Mueller, J. Pavan, H. Schatz, A. Stolz, S. L. Tabor, B. E. Tomlin, and M. Wiedeking, Phys. Rev. C **73**, 044322 (2006).

[66] J. D. Cossairt, R. E. Tribble, and R. A. Kenefick, Phys. Rev. C **15**, 1685 (1977).

[67] D. Ehrlich, Z. Phys. **207**, 268 (1967).

[68] S. C. Gujrathi and S. K. Mukherjee, Phys. Rev. **159**, 909 (1967).

[69] Ph. Dessagne, M. Bernas, M. Langevin, G. C. Morrison, J. Payet, F. Pougheon, and P. Roussel, Nucl. Phys. A **426**, 399 (1984).

[70] M. Bernas, J. C. Peng, H. Doubre, M. Langevin, M. J. Le Vine, F. Pougheon, and P. Roussel, Phys. Rev. C **24**, 756 (1981).

[71] G. T. Hickey, G. M. Crawley, D. C. Weisser, and N. Shikazono, J. Phys. G: Nucl. Phys. **G2**, L143 (1976).

[72] T. S. Bhatia, H. Hafner, R. Haupt, R. Maschuw, and G. J. Wagner, Z. Phys. A **281**, 65 (1977).

[73] R. Haupt, C.-A. Wiedner, G. J. Wagner, K. Wannebo, T. S. Bhatia, H. Hafner, R. Maschuw, W. Saathoff, and S. T. Thornton, Z. Phys. A **317**, 193 (1984).

[74] E.-M. Franz, S. Katcoff, H. A. Smith Jr., and T. E. Ward, Phys. Rev. C **12**, 616 (1975).

[75] R. Knöbel, Ph.D. thesis, Justus-Liebig Universität Gießen, 2008 (unpublished).

[76] L. Gaudefroy, Ph.D. thesis, Université Paris XI Orsay, 2005.

[77] A. Estradé *et al.*, Phys. Rev. Lett. **107**, 172503 (2011).

[78] J. Van Roosbroeck *et al.*, Phys. Rev. Lett. **92**, 112501 (2004).

[79] K. T. Flanagan *et al.*, Phys. Rev. Lett. **103**, 142501 (2009).

[80] B. Cheal *et al.*, Phys. Rev. Lett. **104**, 252502 (2010).

[81] K. T. Flanagan *et al.*, Phys. Rev. C **82**, 041302(R) (2010).

[82] P. Vingerhoets *et al.*, Phys. Rev. C **82**, 064311 (2010).

[83] D. Lunney, J. M. Pearson, and C. Thibault, Rev. Mod. Phys. **75**, 1021 (2003).

[84] M. Bender, G. F. Bertsch, and P.-H. Heenen, Phys. Rev. C **78**, 054312 (2008).

[85] P. Van Isacker, D. D. Warner, and D. S. Brenner, Phys. Rev. Lett. **74**, 4607 (1995).

[86] M. Bender and P.-H. Heenen, Phys. Rev. C **83**, 064319 (2011).

[87] V. A. Kravtsov, Sov. Phys. JETP **14**, 1317 (1962).

[88] N. Zeldes, M. Gronau, and A. Lev, Nucl. Phys. **63**, 1 (1965).

[89] G. Audi, Ph.D. thesis, Université Paris-Sud–Orsay, France, 1981 (unpublished).